EarthArXiv PREPRINT: Oceanic redox conditions during the terminal Cambrian extinction event

Xi Chen[a,b*], Graham A. Shields[b], Morten B. Andersen[c], Chen Qiu[a], Si-Yu Min[a], Qing-Feng Shao[d] and Hong-Fei Ling[a]

[a] *Laboratory for Mineral Deposits Research, School of Earth Sciences and Engineering, Nanjing University, Nanjing 210023, China*

[b] *Department of Earth Sciences, University College London, London WC1E 6BT, UK*

[c] *School of Earth and Environmental Sciences, Cardiff University, Cardiff CF10 3AT, UK*

[d] *Key Laboratory of Virtual Geographic Environment, Nanjing Normal University, Nanjing 210023, China*

This manuscript has been submitted to Chemical Geology on 13 Jan 2022 for peer review. Since May 2022, there has been one complete review, and another pending review.

Author for correspondence:
Xi Chen, Department of Earth Sciences, UCL (x-chen@ucl.ac.uk)

EarthArXiv PREPRINT: Oceanic redox conditions during the terminal Cambrian extinction event

Xi Chen[a,b*], Graham A. Shields[b], Morten B. Andersen[c], Chen Qiu[a], Si-Yu Min[a], Qing-Feng Shao[d] and Hong-Fei Ling[a]

[a] *Laboratory for Mineral Deposits Research, School of Earth Sciences and Engineering, Nanjing University, Nanjing 210023, China*

[b] *Department of Earth Sciences, University College London, London WC1E 6BT, UK*

[c] *School of Earth and Environmental Sciences, Cardiff University, Cardiff CF10 3AT, UK*

[d] *Key Laboratory of Virtual Geographic Environment, Nanjing Normal University, Nanjing 210023, China*

Abstract

Marine animal diversity during the late Cambrian was punctuated by a series of extinctions that have generally been attributed to oceanic anoxic events associated with positive carbon isotope excursions. Here we present carbon and uranium isotope compositions ($\delta^{13}C$ and $\delta^{238}U$) as proxies for organic matter burial and oceanic redox, respectively, from carbonate rocks of the Wa'ergang section, South China. The dataset spans an interval that includes the last major negative $\delta^{13}C$ excursion (TOCE) of the Cambrian Period. The TOCE is a globally documented event, recovery from which corresponds to the terminal Cambrian extinction event. $\delta^{13}C$ and $\delta^{238}U$ values covary through the section, shifting initially to lower values, with $\delta^{238}U$ falling below the modern open-ocean seawater value from the start to the middle of the profile, followed by a shift to higher values towards the end of the Cambrian. The co-occurrence of $\delta^{13}C$ and $\delta^{238}U$ negative excursions, as well as extinctions associated with rising $\delta^{238}U$, has seldom been reported. Here we argue that positive $\delta^{13}C$ vs. $\delta^{238}U$ covariation can be produced by expanded intermediate reducing settings (from low-O_2 suboxia to intermittently sulfidic anoxia), which are likely to have been widespread during the late Cambrian with low atmospheric pO_2 and a greenhouse climate. A stepwise increase in the $\delta^{238}U$ baseline in carbonates across the Ediacaran−Cambrian boundary is consistent with the growing importance of an intermediate reducing sink through this interval. We propose further that divergent trends in deep and upper ocean redox conditions, as

well as the waxing and waning of the accommodation space for organic carbon burial, in response to climate and sea-level changes, could have driven the parallel isotope excursions. An expansion of intermediate reducing conditions, rather than persistent anoxic euxinia, is more consistent with the presence of benthic faunas and shoreward extension of deeper-water fauna that may have had a greater tolerance against hypoxia.

Keywords: uranium isotopes; TOCE; suboxic; OMZ; intermediate reducing; end-Ptychaspid Biomere extinction

1. Introduction

The major body plans (phyla) of animals were already established during the early Cambrian bioradiations ('Cambrian Explosion'), although available marine ecospace would not be filled to capacity until the Late Ordovician (Sheehan, 2001) and animal diversity suffered repeated extinctions after the 'Cambrian Explosion' (Palmer, 1984; Zhuravlev, 2001). Especially, during the Furongian Epoch (497–485.4 Ma, the last Cambrian epoch), marine invertebrate fossil diversity decreased significantly during the so-called 'Furongian Gap' (Harper et al., 2019). This interval comprises three major extinction events separating suprazonal biostratigraphic units named 'biomeres' (Palmer, 1965; Stitt, 1971; Palmer, 1984; Taylor, 2006). Sea-level changes, cooling, upwelling, and anoxic events have all been proposed as possible triggers for those extinctions (Palmer, 1984; Taylor, 2006; Gill et al., 2011; Saltzman et al., 2015).

The youngest Cambrian extinction event, the end-Ptychaspid Biomere extinction, occurred within the last Cambrian stage. Like other end-of-biomere extinctions, it was first recognized on the Laurentian shelf where trilobites experienced major and rapid turnover (Stitt, 1971; Palmer, 1984). This extinction was subsequently shown to also affect conodonts and brachiopods simultaneously (Miller et al., 2006; Freeman et al., 2018). Although there has been lack of paleontological studies on the global occurrences of this specific end-of-biomere extinction, the earlier end-Marjumiid Biomere extinction was observed in China, Australia, and Sweden (Saltzman et al., 2000; Ahlberg et al., 2009). All three late Cambrian extinctions have been noted to be associated with globally correlative carbon isotope excursions (Ripperdan et al., 1992; Saltzman et al., 2011,

2015), confirming their global origins. While the two earlier late Cambrian extinctions are related to the SPICE Event (Steptoean Positive Carbon Isotope Excursion, Saltzman et al., 2000), the last one is related to the TOCE Event (Top Of Cambrian Excursion, Buggisch et al., 2003; Zhu et al., 2006; Peng et al., 2012; Zhu et al., 2021), a negative carbon isotope anomaly that has two synonyms (Zhu et al., 2021): HERB (HEllnmaria–Red Tops Boundary, Ripperdan, 2002; Landing et al., 2020) and SNICE (Sunwaptan Negative Isotope Carbon Excursion, Sial et al., 2013). As with other end-of-biomere extinctions, multiple triggers have been proposed (Westrop and Ludvigsen, 1987; Loch et al., 1993; Runkel et al., 2010), although no clear consensus exists over the cause of either the terminal Cambrian extinction or the TOCE. However, changes in ocean redox conditions may have been a key factor linking those biotic and abiotic events.

In the last decade, uranium isotope compositions ($^{238}U/^{235}U$ ratios; reported as $\delta^{238}U$, the permil variation of $^{238}U/^{235}U$ compared to the standard NBL CRM-145), have been used as a novel ocean redox proxy to investigate relationships between environmental and evolutionary crises (e.g., Dahl et al., 2014, 2019; Lau et al., 2016, 2017; Jost et al., 2017; White et al., 2018; Clarkson et al., 2018; Zhang et al., 2018b, 2019, 2020; del Rey et al., 2020). The redox sensitivity of $\delta^{238}U$ is due to the exchange between the common U species, U(VI) vs. U(IV), and associated U isotope fractionation. In the modern ocean, U exists as the oxidized U(VI) species in stable uranyl bicarbonate complexes and has a long oceanic residence time (ca. 400 kyr) relative to the ocean mixing time (1–2 kyr). As a consequence, its concentration and isotope composition ($\delta^{238}U$) are homogeneously distributed in open-ocean seawater (OSW) (Andersen et al., 2016). While the dissolved riverine U load is the main ocean input, removal may occur as either the oxidized U(VI) or reduced U(IV) species. The largest U sink is U uptake into reducing sediments, where U(VI) is reduced to the largely immobile U(IV) species with a preference for the heavier ^{238}U isotope due to nuclear volume effects (Stirling et al., 2007; Weyer et al., 2008). Although U reduction occurs at a redox potential close to that for iron reduction (i.e., less reducing than 'sulfidic anoxia' or 'euxinia'), and primarily at or below the sediment-water interface (Morford et al., 2005), the observed $^{238}U/^{235}U$ fractionation between sediment and open-ocean seawater ($\Delta_{sed-OSW}$), is greatest under persistently sulfidic bottom waters in semi-restricted basins in modern environments (e.g., Andersen et al., 2014; Cole et al., 2020). Along continental margins, U removal occurs in oxygen-poor

regions under a range of different and 'intermediate' reducing conditions from anoxia within the sediment-porewater interface to low-O_2 suboxic[1] and intermittent sulfidic anoxic conditions (Dunk et al., 2002). Compared with the semi-restricted euxinic U sink, the intermediate reducing sink is associated with only minor expressed $\Delta_{sed-OSW}$, on average, due to various reasons. Firstly, when reductive U removal occurs within sediments beneath suboxic bottom waters, the expressed $\Delta_{sed-OSW}$ can be lowered due to diffusion limitation on the U supply (Weyer et al., 2008; Andersen et al., 2014; Lau et al., 2020). Secondly, both spatial and temporal variations of oxygen minimum zones (OMZ) may lead to non-steady state U uptake and mute the expressed $\Delta_{sed-OSW}$ (Weyer et al., 2008; Andersen et al., 2016; He et al., 2021). Thirdly, particulate non-lithogenic uranium (PNU, Zheng et al., 2002), i.e., organic-matter-related U, can contribute significantly to total authigenic U when the bottom water has low dissolved oxygen content (<25 μM, Zheng et al., 2002). Because PNU is likely depleted in ^{238}U (Holmden et al., 2015; Hinojosa et al., 2016; Abshire et al., 2020), its mixing with U uptake *in situ* within the sediments, enriched in ^{238}U, can mute the total expressed $\Delta_{sed-OSW}$. In contrast, the U sink of U(VI) species is smaller than the reduced U sink (Dunk et al. 2002) and also generally associated with smaller U isotope fractionation, but towards lighter isotope compositions (e.g., Fe–Mn nodules have $^{238}U/^{235}U$ that are ~0.2‰ lower than seawater; Goto et al., 2014). A larger U sink is the U(VI) uptake into carbonates, both via biotic or abiotic pathways. Although, a range of $\delta^{238}U$ values have been observed from modern carbonates, both towards higher and lower $\delta^{238}U$, the majority show little variation from modern seawater (e.g., Weyer et al., 2008; Romaniello et al., 2013; Chen et al., 2016; Clarkson et al., 2020). The observed higher $\delta^{238}U$ values are often attributed to U(IV) incorporation in carbonate cements under reducing porewater conditions, while lower $\delta^{238}U$ may derive from effects of U adsorption and/or organic matter (e.g., Romaniello et al., 2013; Chen et al., 2016; Clarkson et al., 2021). Because carbonates deposited un-

[1] We choose "suboxic" to describe the depositional environments with low-O_2 (without specific upper and lower limits of dissolved O_2) bottom waters, because "hypoxic" (used by Andersen et al., 2017) is for "physiological regime" (Tyson and Pearson, 1991) and its definition depends on the specific organism. All the terms for redox conditions (oxic, suboxic, non-sulfidic anoxic, intermediate redox, sulfidic, euxinic) refer to the bottom waters unless additional specifications, because water column redox conditions are more pertinent to animals.

der oxic conditions show limited U isotope fractionation, marine carbonates are the favored geological archive for estimating the $\delta^{238}U_{OSW}$ in the past (e.g., Weyer et al., 2008; Romaniello et al., 2013; Chen et al., 2016; Clarkson et al., 2020).

The global redox sensitivity of the uranium isotope proxy relates to changing OSW $\delta^{238}U$ values due to the mass-weighted isotope fractionation of the burial flux ($\delta^{238}U_{OSW} = \delta^{238}U_{input} - \sum\Delta_i f_i$, f_i is the proportion for each burial flux) compared to the input. Consequently, geological records of negative $\delta^{238}U$ excursions have been taken to indicate expansion of euxinia (Cole et al., 2020), even though both the modern carbonate and intermediate reducing fluxes contribute a large proportion of the total U sink today compared to euxinic semi-restricted basins (Dunk et al. 2002; Andersen et al., 2016, 2017; Cole et al., 2020). Alternatively, we argue here that muted or positive excursions of $\delta^{238}U$ could relate instead to expansion of the intermediate reducing sink at the expense of the euxinic sink and/or expansion of the oxic sink.

This study presents uranium and carbon isotope profiles and metal concentrations of marine limestones spanning the full TOCE interval at the Wa'ergang section in South China, in order to study the coupling between oceanic redox conditions and the global carbon cycle during the late Cambrian, with implications for improved understanding of the terminal Cambrian extinction event.

2. Materials and methods

The Wa'ergang section is situated in Taoyuan County, western Hunan Province, China. It is located on the Jiangnan Slope on the southeastern margin of the Yangtze Platform (Fig. 1B). At the end of the Cambrian Period, the Yangtze plate was located on the northern margin of the Gondwana continent. The middle to upper Cambrian strata were continuously deposited in the studied area, and are mainly composed of richly fossiliferous carbonate rocks with stratigraphically useful assemblages of conodonts and trilobites (Peng et al., 2014; Bagnoli et al., 2017; Dong and Zhang, 2017). The basin should have been well connected to the open ocean because the section contains a rich assemblage of cosmopolitan trilobites that can be used for intercontinental correlation (Peng et al., 2012, 2014).

A total of 32 dark-gray limestone samples spanning the TOCE Event were collected from the upper part of Shenjiawan Formation at the Wa'ergang section. Our sampling was interrupted by a possibly allochthonous massive carbonate debris bed (~3 m), and this bed marks the approximate boundary between the *Eoconodontus* and *Cordylodus proavus* conodont zones (Bagnoli et al., 2017) and also the end-Ptychaspid Biomere extinction horizon (see section 4.4 for more details). The Wa'ergang section above this bed is not as continuous as below, and so previous biostratigraphic (Bagnoli et al., 2017) and carbon isotope chemostratigraphic (Li et al., 2017) studies also stopped around this level. Fine-grained, micritic limestones without secondary veins and recrystallization were finely powdered. 50–150 μg powder of each sample was reacted with phosphoric acid at 70 °C in a Kiel IV carbonate device, and the CO_2 generated was analyzed on a MAT 253 mass spectrometer in the Nanjing Institute of Geology and Palaeontology, Chinese Academy of Sciences. Both $\delta^{13}C$ and $\delta^{18}O$ values are reported relative to the V-PDB. The long-term external reproducibilities of $\delta^{13}C$ and $\delta^{18}O$ analyses are ±0.04‰ and ±0.08‰, respectively (1 SD, 600 replicates during one year of the laboratory standard GBW-04405). Metal concentration and U isotope analyses were carried out using an ELEMENT XR ICP-MS (Nanjing University) and NEPTUNE Plus MC-ICP-MS (Nanjing Normal University), respectively. Samples (~100 mg) were leached by agitation for 4 to 12 hours in 1 M HCl at room temperature, until no further effervescence was observed (Lau et al., 2016; Zhang et al., 2018a). The sample supernatant was separated from the remaining residue. A small aliquot was taken and diluted 500-fold for each sample prior to the metal analyses. Rhodium (Rh) was added as internal standard for analyses (samples and standards). Concentration of each metal was calculated by comparison of the ^{103}Rh-normalized intensity of a sample with that of an artificial standard with high Ca and Mg contents similar to carbonates. The remaining sample was spiked with the IRMM-3636 ^{236}U–^{233}U double spike, aiming for a $^{236}U/^{235}U$ ratio of ~4 before preparation for U purification. The U purification from matrix elements were done using RE resin following published protocols used to successfully separate U from a range different matrix including carbonates (Bura-Nakić et al., 2018, 2020; Clarkson et al., 2020) and subsequently dissolved in 2% (v/v) HCl aiming for ~50 ppb U for mass spectrometric measurements. Full procedural blanks were <0.1 ng U, negligible to the sample sizes measured. Uranium isotope measurements were performed in a static collection with 10^{11} Ω resistors on all Faraday cups. Corrections of ^{238}U and ^{235}U impurities (from IRMM-3636), tailing, hydrate formation and mass

bias corrections were carried out as described by Andersen et al. (2016). The $\delta^{238}U$ values were measured relative to the NBL CRM-145 standard. The internal precisions (2 SE) on measured $\delta^{238}U$ values are better than ±0.05‰ for all samples. Consecutive measurements of the in-house CZ-1 uraninite standard gave $\delta^{238}U$ = −0.04 ± 0.06‰ (2 SD, 45 replicates during two years), in excellent agreement with the obtained values for the same standard from different laboratories and analytical set-ups (e.g., Stirling et al., 2007; Andersen et al., 2014, 2016; Bura-Nakić et al., 2018; Clarkson et al., 2020). Further, analyses of the IAPSO seawater gave $\delta^{238}U$ −0.38 ± 0.04‰ (2 SD, n = 3) within error of other determinations of this standard (Holmden et al., 2015).

3. Results

The $\delta^{13}C$ values from Wa'ergang section range between 0.15‰ and 2.43‰, and the $\delta^{18}O$ values lie within a narrow range (−10.2 to −8.8‰). The $\delta^{13}C$ profile exhibits a negative excursion in the middle (Fig. 1C). There is no covariation between $\delta^{18}C$ versus $\delta^{18}O$ or Mn/Sr (Fig. 2A, 2B).

The $\delta^{238}U$ data ranges between −0.66‰ and −0.14‰ and shows a depth profile (from 745 m to 875 m) that mimics the $\delta^{13}C$ trend, with a near synchronous negative excursion. Values decrease from −0.14‰ to a nadir of −0.66‰ in the middle (at 815 m), and then return to near initial values (−0.23‰) at the end of the TOCE Event (Fig. 1C). The Ca-normalized U concentration (U/Ca, μmol/mol) ranges between 0.52 and 3.22 (Fig. 1C, 2D). The highest U/Ca ratios are observed at the very beginning and end of the depth profile, whereby the four samples with the highest U/Ca ratios also exhibit the highest $\delta^{238}U$ values. The U/Ca ratios, excluding those four samples, distribute in two groups clustering around 0.8 and 1.5, respectively (Fig. 2D), and show weak correlation with $\delta^{238}U$ values largely due to U/Ca ratios clustering around 1.5. There is no correlation with $\delta^{238}U$ values for the other samples having U/Ca ratios clustering around 0.8, and the range and trend of $\delta^{238}U$ curve exhibited by these samples remains the same as all the samples. The U/Al (ppm/ppm) ratios in the carbonate leachates range from 1.43×10^{-4} to 1.54×10^{-3}. Neither U contents nor U isotope compositions covary with Al concentrations (with correlation coefficients $R^2 < 0.06$ and *t*-test *p*-values > 0.33).

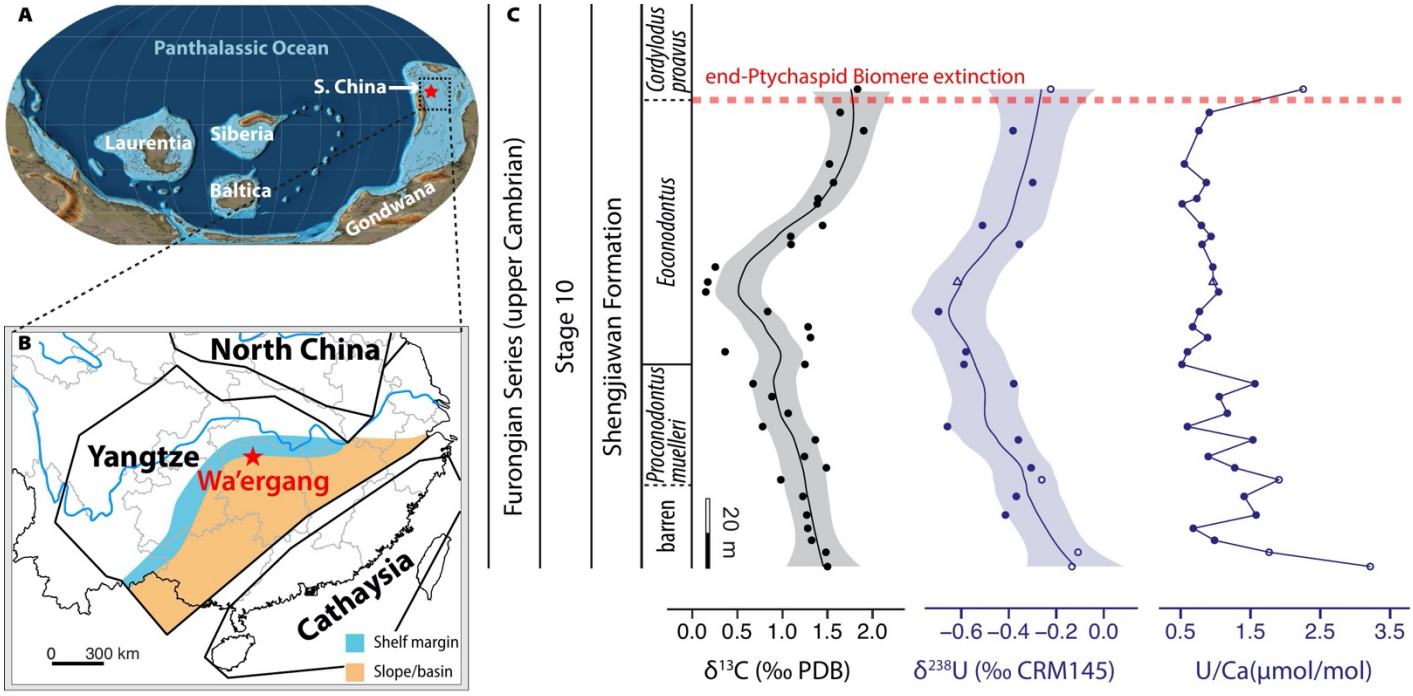

Figure 1: A: Paleogeographic map showing South China and other paleocontinents during the late Cambrian (Scotese, 2021). The red star marks Wa'ergang section. B: Simplified geological map of South China and the location of Wa'ergang section on the southeastern margin of the Yangtze plate. C: Chemostratigraphic data (carbon and uranium isotope compositions) of late Cambrian succession from Wa'ergang section in Taoyuan County, western Hunan Province, China. The $\delta^{238}U$ data possibly being affected by dolomitization or reducing porewater are denoted by a triangle and open circles, respectively. The $\delta^{238}U$ data are corrected for detrital U contributions. Curves of $\delta^{238}U$ and $\delta^{13}C$ are smoothed by LOESS fitting with shaded 95% confidence intervals. A red dashed line right below a carbonate debris bed marks the boundary between the *Eoconodontus* and *Cordylodus proavus* conodont zones (Bagnoli et al., 2017), and this biozone boundary corresponds to the rising limb of the TOCE (Landing et al., 2011; Saltzman et al., 2015; Li et al., 2017; Azmy, 2019) and the terminal Cambrian end-Ptychaspid Biomere extinction event (Palmer, 1984; Landing et al., 2011).

4. Discussion

4.1. Assessment of the isotope data

There are a range of considerations for the obtained isotope data that require evaluation. It is particularly important to demonstrate how likely measured data show primary marine signatures or are altered by various syngenetic, diagenetic or mixing effects.

Diagenetic alteration of carbonates, by interaction with meteoric waters, tends to deplete Sr and ^{18}O but enrich Mn. Because carbon is a major element in carbonates but minor in meteoric waters, its isotope composi-

193 tion is less easily altered compared with Sr and O. Limestones with Mn/Sr ratios lower than 10 are consid-
194 ered most likely to preserve primary $\delta^{13}C$ values (Kaufman and Knoll, 1995). In our dataset, Mn/Sr ratios are
195 all lower than 0.7, which is even lower than a proposed upper limit of 2 for preserving primary Sr isotope
196 compositions (Kaufman and Knoll, 1995). The $\delta^{18}O$ values do not correlate with Sr, Mn, or Mn/Sr (with cor-
197 relation coefficients $R^2 < 0.09$ and *t*-test *p*-values > 0.11), suggesting that $\delta^{18}O$ values are also not obviously
198 altered. Moreover, neither $\delta^{18}O$ nor Mn/Sr, as diagenetic proxies, vary systematically with changes in $\delta^{13}C$
199 ($R^2 < 0.06$ and *p*-values > 0.19), which strongly supports use of these carbon isotope data for interpreting the
200 paleoceanic environment.

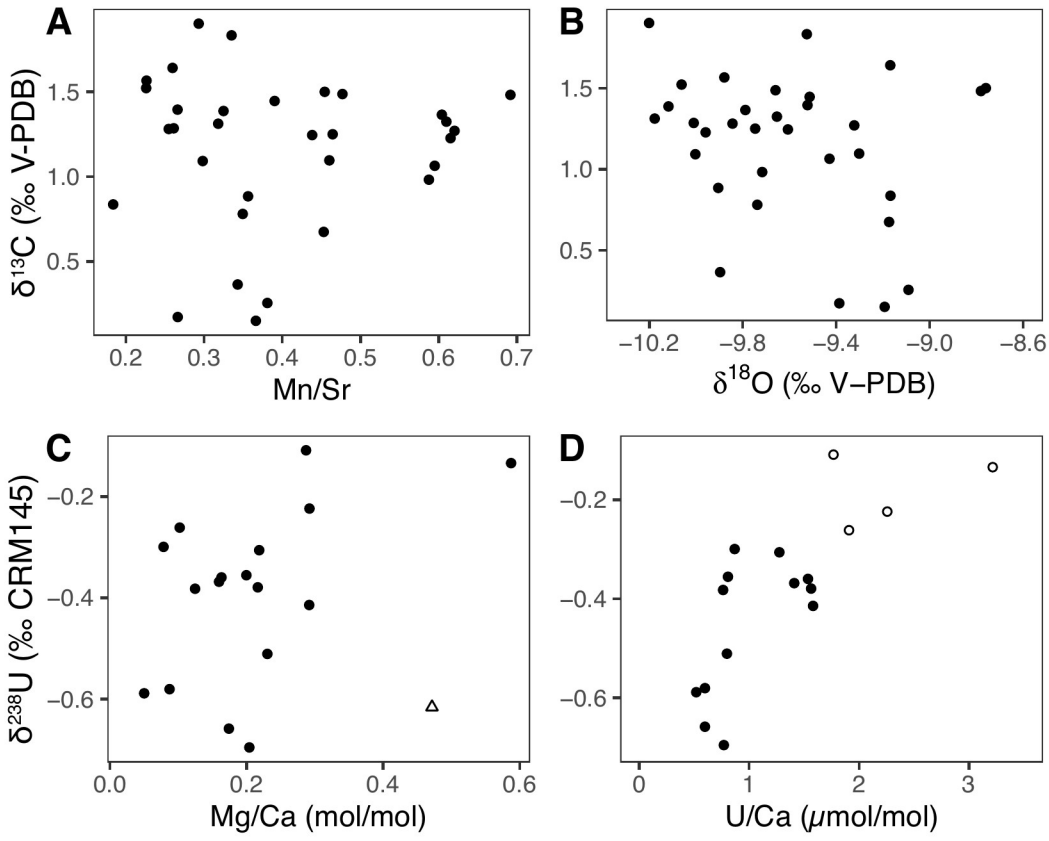

201

202 Figure 2: Cross plots of $\delta^{13}C$ vs. proxies for diagenetic alteration (A: Mn/Sr ratio, B: $\delta^{18}O$), and $\delta^{238}U$ vs.
203 proxies for dolomitization (shift $\delta^{238}U$ to lower values, C: Mg/Ca molar ratio) and reducing porewater (shift
204 $\delta^{238}U$ to higher values, D: U/Ca) in limestone samples from Wa'ergang section. The data possibly being af-
205 fected by dolomitization or reducing porewater are denoted by a triangle (low $\delta^{238}U$ and high Mg/Ca) and
206 open circles (high $\delta^{238}U$ and high U/Ca), respectively.

207 For the U isotope systematics, the potential effects of detrital contribution, U isotope fractionation mecha-
208 nisms and diagenesis all require discussion. In terms of detrital contribution, the Al content in carbonate
209 leachates may be related to trace levels of detrital siliciclastic rock components that may dissolve during the

210 leaching (e.g., Clarkson et al., 2020) and can therefore be used to assess siliciclastic contamination of the
211 leachates. Assuming that the Al is solely related to the detrital siliciclastic contribution, it is possible to cor-
212 rect the bulk $\delta^{238}U$ values for this by mass balance, based on assumptions about the U/Al and $\delta^{238}U$ of this
213 phase. Assuming U/Al = 3.5×10^{-5} (ppm/ppm; McLennan, 2001) and $\delta^{238}U = -0.3‰$ (Andersen et al., 2014)
214 for the detrital contribution results in a shift in measured $\delta^{238}U$ less than 0.072‰, indicating that any effect
215 from detrital U would be negligible in these limestone leachates. Similarly, Clarkson et al. (2020) performed
216 leaching experiments on carbonates using different leaching reagents showed no bias in the obtained $\delta^{238}U$
217 using 1 N HCl compared to a range of other milder leaching methods.

218 There are several syngenetic or diagenetic effects that may affect the $\delta^{238}U$ in carbonates. Carbonate $\delta^{238}U$
219 values can shift to lower values during dolomitization, especially when molar Mg/Ca ratios are higher than
220 ca. 0.5 (Romaniello et al., 2013). However, data from upper Jurassic carbonates do not show any correlation
221 between the degree of dolomitization (Mg/Ca) and $\delta^{238}U$ values (Herrmann et al., 2018), which is also true
222 for our samples ($R^2 = 0.10$, *p*-value = 0.21, and see Fig. 2C). Our samples with low $\delta^{238}U$ values (<−0.6‰)
223 generally have low Mg/Ca molar ratios (<0.21), with only one exception whose Mg/Ca molar ratio is 0.47
224 (denoted by a triangle in Fig. 1C and Fig. 2C). In contrast, the authigenic uptake of additional U under reduc-
225 ing conditions can shift $\delta^{238}U$ to higher values. This effect is likely to result dominantly from uptake of re-
226 duced U into carbonate-cements under reducing pore-water conditions (e.g., Romaniello et al., 2013; Clark-
227 son et al., 2021). It is striking that the four samples with the highest $\delta^{238}U$ values also have the highest U con-
228 tents (see Fig. 2D). This suggests that they may have been affected by authigenic uptake of U under reducing
229 conditions, analogous to modern Bahamian carbonates (Romaniello et al., 2013). In Eocene carbonate sam-
230 ples, Clarkson et al. (2021) did observe the effect of reduced U uptake and higher $\delta^{238}U$ with increasing
231 U/Ca, whereby the increase initiated at >0.125 (μmol/mol) in those samples. While the exact U/Ca threshold
232 in Clarkson et al. (2021) cannot be used in our case due to different oceanographic settings and ocean U
233 budgets, we argue that these four U-rich samples, towards the base and top of the depth profile, might record

234 higher $\delta^{238}U$ than contemporaneous seawater. For the remaining samples with U/Ca < 1.6, there is no obvi-
235 ous trend of increasing U concentration with high $\delta^{238}U$ (Fig 2D) and so their measured $\delta^{238}U$ values are con-
236 sidered likely to reflect a near seawater $\delta^{238}U$ value at the time of carbonate formation.

237 ## 4.2. The TOCE Event: a global negative carbon isotope excursion

238 The negative $\delta^{13}C$ TOCE excursion has been well-documented in nearly all late Cambrian paleocontinents,
239 including organic carbon isotope profiles in Baltica, and carbonate carbon isotope profiles in western Lau-
240 rentia, northeastern Laurentia, Precordillera terrane, Siberia, Australia, Tarim, North China and South China
241 (Miller et al., 2015; Azmy, 2019; Landing et al., 2020; Zhu et al., 2021). The amplitude of this $\delta^{13}C$ shift
242 ranges between −0.5‰ and −4‰. The nadir of TOCE consistently occurs within the lower part of the *Eoco-*
243 *nodontus* Zone in most of the above-mentioned paleocontinents with sections having well-established bi-
244 ozones (Landing et al., 2011; Azmy, 2019; Landing et al., 2020). Our data from Wa'ergang section show that
245 the onset of the full TOCE Event lies within the *Proconodontus muelleri* Zone, which is also true for Black
246 Mountain in Australia (Ripperdan et al., 1992) and Sneakover Pass in Utah, USA (Miller et al., 2015). The
247 intercontinentally correlative TOCE excursion implies a perturbation of the global carbon cycle.

248 There is still no clear consensus on the cause of TOCE, but it may be linked to sea-level changes. The associ-
249 ation between the $\delta^{13}C$ minimum of TOCE and a regression event is evidenced from disconformities and de-
250 tailed sequence stratigraphic analysis on various paleocontinents, including Australia (Ripperdan et al.,
251 1992), North China (Ripperdan et al., 1993) and Laurentia (Miller et al., 2015). Ripperdan (2002) proposed
252 that weathering of 'old carbon' on formerly productive platforms provided the source of isotopically light
253 carbon. However, weathering of both organic matter and carbonate would have increased after a sea level
254 fall. Furthermore, there is no evidence of widespread shallow water organic rich sediments in the underlying
255 strata, instead, carbonate was deposited in broad tropical epicontinental (epeiric) seas throughout the late
256 Cambrian (Landing, 2011). Therefore, enhanced weathering would have provided isotopically heavy rather
257 than light carbon. We suggest that the TOCE Event could have been driven by changes to carbon sinks rather
258 than sources (see detailed discussions in section 4.4 and 4.5).

4.3. Positive carbon and uranium isotope shifts and the terminal Cambrian extinction

The late Cambrian (Furongian Series) records three extinction events at the top of the Marjumiid, Pterocephaliid, and Ptychaspid biomeres, respectively (Palmer, 1984). The youngest one, the end-Ptychaspid Biomere extinction, coincides precisely with the *Eoconodontus–Cordylodus proavus* conodont Zone boundary (Palmer, 1984; Landing et al., 2011). This biostratigraphic level corresponds to the rising limb of the TOCE, i.e., a $\delta^{13}C$ positive shift following the TOCE nadir (Landing et al., 2011; Saltzman et al., 2015; Li et al., 2017; Azmy, 2019).

Generally, there is evidence against sea-level changes as the 'killing mechanism' of the late Cambrian end-of-biomere extinctions: 1) The lithological changes associated with all three end-of-biomere extinctions are not uniform in different locations, and are usually minimal, although obvious faunal turnovers are similar. 2) Well-defined continent-wide regressions occurred *within* the Pterocephaliid and Ptychaspid biomeres without obvious faunal effects (Palmer, 1984; Loch et al., 1993; Taylor, 2006). Specifically, the link between sea-level (and/or climate) changes and the end-Ptychaspid extinction is highly controversial (Westrop and Ludvigsen, 1987, cf. comments by Loch et al., 1993 and Taylor, 2006; Runkel et al., 2010, cf. comments by Landing, 2011). In contrast, positive $\delta^{13}C$ excursions are strongly related with recurring extinctions from the late Cambrian Furongian Stage to Early Ordovician Tremadocian Stage, providing evidence of periodic expansions of anoxia delaying further animal diversification (Saltzman et al., 1995, 2011, 2015). Coincidence of positive $\delta^{34}S$ shifts at the tops of Marjumiid (Gill et al., 2011) and Symphysurinid (Saltzman et al., 2015) biomeres, and a negative $\delta^{238}U$ shift at the top of the Marjumiid biomere (equivalent to the onset of SPICE, Dahl et al., 2014), provide further evidence for anoxia. However, there has been no strong evidence for anoxia linked with all the other biomeres. Moreover, a negative shift (end-Marjumiid, Dahl et al., 2014), positive shift (end-Ptychaspid, this study), and fluctuation (end-Pterocephaliid, Dahl et al., 2014) of $\delta^{238}U$ have all been observed during the end-of-biomere extinctions, which appears to weaken the proposed link between end-of-biomere extinctions and anoxia.

283 Both positive and negative $\delta^{13}C$ shifts are observed to be associated with negative $\delta^{238}U$ shifts indicating an-
284 oxia during other extinction events or delayed biotic diversifications/recoveries. Broad coincidence of a posi-
285 tive $\delta^{13}C$ shift with a negative $\delta^{238}U$ shift was observed from late Ediacaran (Zhang et al., 2018b), early and
286 late Cambrian (Dahl et al., 2014, 2019), late Silurian (del Rey et al., 2020), Late Devonian (White et al.,
287 2018), Early Triassic (Lau et al., 2016), earliest Jurassic (Jost et al., 2017), and mid-Cretaceous (Clarkson et
288 al., 2018) successions, which is commonly explained by enhanced organic carbon (^{13}C-depleted) burial due
289 to expansion of anoxia (with ^{238}U-enriched sediments). In comparison, negative shifts of both $\delta^{13}C$ and $\delta^{238}U$
290 have been reported less commonly, from Cryogenian (Lau et al., 2017), end-Permian to earliest Triassic
291 (Zhang et al., 2020), Early Triassic (Zhang et al., 2019), and Triassic/Jurassic boundary (Jost et al., 2017)
292 successions. This type of correlation has been attributed to anoxia caused by the release of isotopically light
293 carbon sourced from volcanic degassing and/or decomposition of sedimentary or oceanic organic carbon res-
294 ervoirs. In other words, changes in the global carbon cycle, as proxied by $\delta^{13}C$ shifts, are regarded as the
295 cause in the latter situation, rather than the result of anoxic events as in the former situation. As a special
296 case, isotopically light C emissions during the mid-Cretaceous OAE2 accompanied insignificant negative
297 $\delta^{13}C$ shifts, but induced pronounced and prolonged anoxia as reflected by positive $\delta^{13}C$ shifts and negative
298 $\delta^{238}U$ shifts (Clarkson et al., 2018).

299 Positive $\delta^{238}U$ shifts follow negative shifts through most $\delta^{238}U$ 'excursions' (contra: Lau et al., 2017), indi-
300 cating the waning of anoxia after a perturbation. During a positive $\delta^{13}C$ excursion, a positive $\delta^{238}U$ shift usu-
301 ally corresponds to the recovery/falling limb of the $\delta^{13}C$ excursion (e.g., del Rey et al., 2020; White et al.,
302 2018; Lau et al., 2016; Jost et al., 2017; Clarkson et al., 2018). However, during a negative $\delta^{13}C$ excursion, a
303 positive $\delta^{238}U$ shift can simply correspond to the recovery/rising limb of the $\delta^{13}C$ excursion (Zhang et al.,
304 2020), or lag behind a subsequent positive $\delta^{13}C$ shift due to sustained anoxia (i.e., corresponds to the recov-
305 ery/falling limb of the secondary positive $\delta^{13}C$ excursion, e.g., Jost et al., 2017; Clarkson et al., 2018), or be
306 absent due to even more prolonged anoxia (Lau et al., 2017). Therefore, cases with coeval positive shifts of
307 both $\delta^{13}C$ and $\delta^{238}U$ are rare. Besides the aforementioned one case with nearly synchronous recoveries of C
308 and U isotope data during negative $\delta^{13}C$ excursions (Zhang et al., 2020), positive $\delta^{238}U$ shifts have also been

observed during ongoing positive $\delta^{13}C$ shifts (Dahl et al., 2014; Clarkson et al., 2018). It is plausible that the latter cases may have resulted from a smaller oceanic reservoir of U than C, so that $\delta^{238}U$ responded more rapidly than $\delta^{13}C$ in dynamic states when anoxia waned (Dahl et al., 2014; Clarkson et al., 2018). However, this 'reservoir effect' is inconsistent with similar decay timescales for $\delta^{13}C$ and $\delta^{238}U$ excursions during the SPICE, which implies that other control factors than extent of anoxia may have existed (Dahl et al., 2014).

Nearly synchronous negative excursions (including both falling and rising limbs) of $\delta^{13}C$ and $\delta^{238}U$, as we observe for TOCE, are indeed rare (e.g., Zhang et al., 2020). Besides, all the aforementioned cases with negative shifts of both $\delta^{13}C$ and $\delta^{238}U$ are likely related to warming and anoxia (Lau et al., 2017; Jost et al., 2017; Zhang et al., 2019, 2020), while the falling limb of TOCE has been linked to sea-level fall and therefore cooling. Almost all the aforementioned negative $\delta^{238}U$ shifts are also accompanied by the deleterious effects of anoxia on animals (contra: Tostevin et al., 2019), but the terminal Cambrian extinction is above the nadir of TOCE and coincident with a positive $\delta^{238}U$ shift indicating oxygenation. These unusual features of the TOCE Event could be explained by significant abiotic and biotic roles played by intermediate reducing conditions, as discussed in the following three sub-sections.

4.4. Positive $\delta^{13}C$ vs. $\delta^{238}U$ correlation corroborated by intermediate reducing settings

The seawater $\delta^{13}C$ value is proportional to the relative fraction of carbon buried as organic matter when there are no significant changes in the sources. In modern oceans, ~80% of organic carbon is buried in deltaic sediments and mainly of terrestrial origin (Schlesinger and Melack, 1981; Berner, 1982). The deltaic sink of the late Cambrian would have been significantly reduced because of the lack of land plants. If we omit this sink, the euxinic organic C sink comprises only <5% of the total, whereas about half of organic C burial occurs in intermediate reducing settings (Berner, 1982). By comparison, U isotopic fractionation is most significant in euxinic settings, while muted in intermediate reducing settings (see Section 1 and following discussions). Therefore, $\delta^{238}U$ is a proxy for the extent of persistent sulfidic anoxia, and is highly sensitive because a disproportionately large fraction (~24%) of reduced U is buried in modern euxinic settings accounts for only <0.1% of global sea-floor area (Dunk et al., 2002; Andersen et al., 2016). As similarly proposed by Dahl

et al. (2014), although a negative $\delta^{238}U$ still requires expansion of anoxia, larger contributions from intermediate reducing settings (vs. deltaic sediments in Dahl et al., 2014) for both C and U burial can corroborate the positive $\delta^{13}C$ vs. $\delta^{238}U$ correlation, as we observed throughout the TOCE Event. Such intermediate reducing settings could have been common in late Cambrian oceans.

Redox reconstruction of a continental margin transect provides evidence for the early Cambrian establishment of modern-type OMZs dominated by ferruginous conditions and surrounded by oxic waters (Guilbaud et al., 2018). The persistence of small carbonaceous fossils within the Baltic OMZ suggests that the OMZ oscillated between oxic and ferruginous conditions (Guilbaud et al., 2018). Such specific and dynamic oceanic redox conditions are likely to lead to muted expressed average $\Delta_{sed-OSW}$ (Weyer et al., 2008; Cole et al., 2020; He et al., 2021). The occurrence of such dynamic OMZs could have increased in the late Cambrian due to the progressive warming that occurred since the early Cambrian (Frakes et al., 1992), and therefore their impacts on U and C budgets could have also been enhanced. The sea-level controlled changes in intersection areas of OMZs and continental margins (Lau et al., 2016) would have enhanced the coupling between $\delta^{13}C$ and $\delta^{238}U$.

Low atmospheric pO_2 (ca. 50% present atmospheric level, Krause et al., 2018), together with low O_2 solubility in a typical greenhouse climate (Berner, 1990; Frakes et al., 1992; Trotter et al., 2008; Landing, 2012), would have suppressed the dissolved-oxygen level in the surface ocean seawater during the late Cambrian. Furthermore, there is no unambiguous evidence for late Cambrian polar ice caps, and thus modern-like thermohaline circulation ventilating the deep ocean may not have existed then (Landing, 2012). Saline seawater with low O_2 concentration from lower latitude marginal seas may have contributed to the deep ocean seawater, leading to halothermal instead of thermohaline circulation (Brass et al., 1982; Railsback et al., 1990). Therefore, redox conditions with suboxic bottom waters and underlying anoxic sediments could have been more expansive in both shallow epeiric/marginal and deep open oceans, rather than mainly confined within highly productive continental shelves like today (ca. 6% of modern sea-floor area, Andersen et al., 2016). It is noteworthy that eukaryote-dominated “aquatic bioturbation” may have suppressed persistent euxinia and maintained the ventilation of the deep ocean since the early Cambrian (Butterfield, 2018), even when suboxic

360 waters may have expanded due to above mentioned physical causes. In contrast to the marginal OMZs, such
361 deep ocean suboxic conditions could have been more stable, although the effective $\Delta_{sed-OSW}$ could potentially
362 have been diffusion-limited because of reductive U removal within the sediments under suboxic waters
363 (Weyer et al., 2008; Andersen et al., 2014; Lau et al., 2020).

364 Under both of the above two intermediate reducing settings, organic-related PNU may have been high, even
365 in pelagic settings because of higher preservation potential for the 'marine snow' in a less-oxygenated ocean
366 than today. Moreover, because PNU is likely depleted in ^{238}U (Holmden et al., 2015; Hinojosa et al., 2016;
367 Abshire et al., 2020), the coupling between organic-related PNU and intermediate reducing conditions could
368 further corroborate the positive $\delta^{13}C$ vs. $\delta^{238}U$ correlation.

369 To test the potential of the intermediate reducing U sink as a key driver of oceanic $\delta^{238}U$, we utilize a simple
370 semi-quantitative mass balance model to evaluate the impact of intermediate reducing settings on the global
371 U cycle. Firstly, the duration and magnitude of the $\delta^{238}U$ excursion during TOCE Event have to be estimated.
372 The whole excursion, including both decreasing and rising limbs, spans about two conodont zones, or half of
373 Cambrian Stage 10 (489.5–485.4 Ma), which suggests a duration of ca. 2 Myr. Because the starting and end-
374 ing levels of the $\delta^{238}U$ dataset likely have been impacted by incorporation of reduced U, we choose the low-
375 est sample with relatively low U/Ca, and use its $\delta^{238}U_{carb}$ value (−0.41‰) as the starting level for $\delta^{238}U_{OSW}$.
376 For the sake of simplification, we consider that the studied interval ends at the same level as indicated by the
377 overall $\delta^{238}U_{carb}$ trend.

378 Table 1: Parameters used in U mass balance modeling.

Parameter	Value
U concentration[1] and isotope composition[2] in modern open-ocean seawater	3.238 ppb, −0.39‰
Total volume of the ocean	1.37×10^{21} L
Total area of ocean floor	3.61×10^{14} m^2
Modern rate of U output flux and isotope fractionation[2]:	
Euxinic	1.130×10^{-3} g m^{-2} yr^{-1}, 0.42‰
Intermediate reducing	2.088×10^{-4} g m^{-2} yr^{-1}, 0.15‰
Carbonates (oxic)	1.158×10^{-4} g m^{-2} yr^{-1}, 0‰
Metalliferous (oxic)	7.121×10^{-7} g m^{-2} yr^{-1}, −0.25‰
Modern U output flux and isotope fractionation: hydrothermal[2, 3]	6×10^6 mol, 0.25‰
Modern total U input flux and isotope composition[2, 4]	45×10^6 mol, −0.246‰

(1) Chen et al. (1986); (2) based on U output flux and areal fraction of each redox setting estimated by Andersen et al. (2016); (3) assume constant values; (4) assume steady state of modern marine ^{238}U–^{235}U budget.

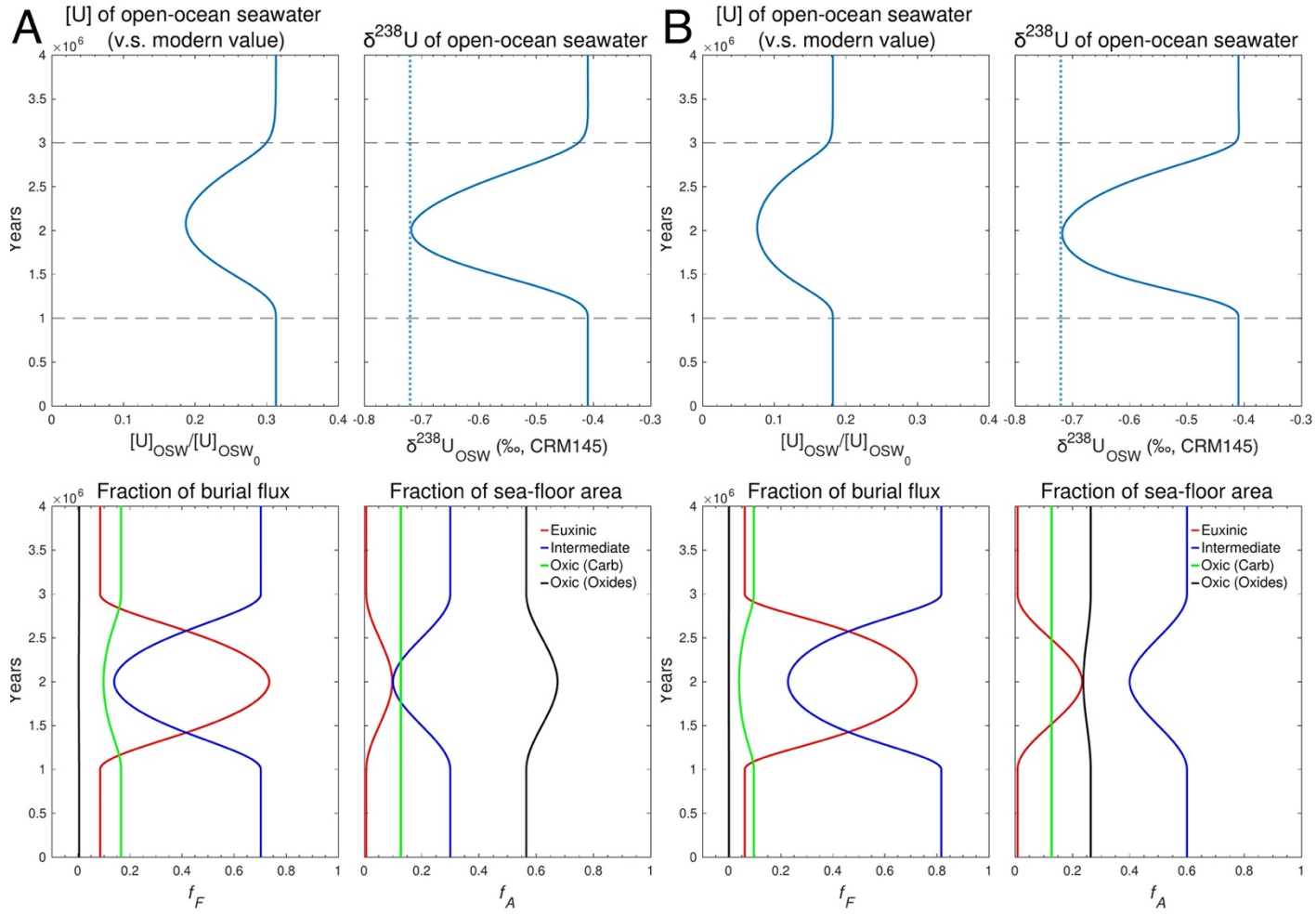

Figure 3: The results of simple semi-quantitative mass balance modeling for the evolution of open-ocean seawater (OSW) $\delta^{238}U$ under two scenarios of changing intermediate reducing and euxinic areas during the terminal Cambrian. The initial f^{A}_{inter} is 30% and 60% in scenarios A and B, respectively, and it evolves to decrease by 20% in both scenarios. The oxic areal extent of carbonate deposits is held constant. This modeling mainly demonstrates: 1) An obtained $\delta^{238}U_{OSW}$ value could accommodate various combinations of proportions of redox conditions; 2) A scenario with higher f^{A}_{inter} has a smaller oceanic U reservoir; 3) How [U] and $\delta^{238}U$ of OSW respond to changes in negatively correlated f^{A}_{eux} and f^{A}_{inter}, and the magnitude of increase in f^{A}_{eux} could be less than the magnitude of decrease in f^{A}_{inter} (scenario A).

In the modern, the intermediate reducing sink of U has a lower burial rate and a smaller average isotope fractionation factor ($\Delta_{inter-OSW} \approx +0.15‰$) than the euxinic sink (cf. typical $\Delta_{eux-OSW}$ is between +0.4‰ and +0.6‰, Andersen et al., 2014; Cole et al., 2020). Combining those two factors, a greater areal fraction of the intermediate reducing settings (f^{A}_{inter}) at the cost of euxinic settings (f^{A}_{eux}) would have increased both the ocean U reservoir and the $\delta^{238}U_{OSW}$, and vice versa, as demonstrated in the modeled oceanic U evolution through time in Fig. 3. An obtained $\delta^{238}U_{OSW}$ value could accommodate various combinations of proportions

of redox conditions, as demonstrated by modeling scenario A versus B in Fig. 3. A scenario with a higher f^{A}_{inter} has a smaller oceanic U reservoir. For example, obtaining a $\delta^{238}U_{OSW}$ of −0.41‰, as used as the initial state, scenario B with a higher f^{A}_{inter} (60%) than scenario A (30%), it induces a lower $[U]_{OSW}$ for scenario B than A (18% vs. 31% of modern level for A and B, respectively). Therefore, even if the $\delta^{238}U_{OSW}$ was similar to the modern value, the oceanic U reservoir could have been smaller and probably more sensitive to changes in oceanic redox state during times when intermediate reducing settings were more expansive (scenario B vs. A, or late Cambrian vs. modern).

Obviously, the modeling has some caveats including the definition and choice of set values of the parameters used (listed in Table 1). However, our main purpose here is to illustrate how different changes in the relative proportions of intermediate reducing and euxinic U sinks can drive the same observed shifts in $\delta^{238}U$, and to highlight the importance of the intermediate reducing sink in minimizing the oceanic U reservoir and inducing positive $\delta^{238}U$ shifts. An overall increasing size of the intermediate reducing U sink, including modern-type dynamic OMZ settings and persistently suboxic settings overlying anoxic sediments, should create a higher $\delta^{238}U$ baseline than an ocean dominated by a sustained euxinic sink. Plotting a compilation of available carbonate $\delta^{238}U$ data from late Ediacaran to Cambrian times (Fig. 4) shows, despite considerable variability in the data, a higher $\delta^{238}U$ baseline (reflected in median, mean, and nadirs of negative excursions) during the Cambrian than the Ediacaran. The $\delta^{238}U$ data from this study are consistent with this higher baseline.

4.5. Plausible climatic and oceanic drivers

Unlike all the reported cases with covarying negative $\delta^{13}C$ and $\delta^{238}U$ shifts (Lau et al., 2017; Jost et al., 2017; Zhang et al., 2019, 2020), there is no evidence for either significant injection of isotopically light carbon (e.g., volcanic degassing, oxidization of methane hydrates or DIC pool) or warming during the TOCE Event. Although weathering of 'old carbon' may have contributed to the negative $\delta^{13}C$ shift, it is unlikely that those recalcitrant sedimentary carbon could have significantly increased the atmosphere pCO_2 and global temperature. On the contrary, as mentioned in section 4.2, there is evidence for sea-level fall and thus cooling associated with the TOCE nadir.

With generally high pCO_2 levels, the relationship between the extent of anoxia and pCO_2 is highly non-linear, and both cooling and warming can induce expansion of anoxia (modeling results shown in Fig. 2 of Pohl et al., 2021). The trends for deep and upper ocean redox conditions in response to cooling can be divergent, such as the cases of the last glacial maximum (LGM, Jaccard and Galbraith, 2012) and end-Ordovician (Bartlett et al., 2018; Pohl et al., 2021). Cooling increases oxygen solubility and oxygenates the upper ocean (<1500 m, Riedinger et al., 2021). However, less efficient ocean circulation transporting oxygen to depth (i.e., ventilation) and/or slowing down of the degradation of sinking organic matter (i.e., biological pump) could deoxygenate the deep ocean (Sigman et al., 2010; Matsumoto, 2007). Therefore, we prefer scenario A in Fig. 3 as better fitting the ocean redox changes during the TOCE Event, with a spread of both anoxic (possibly in deep ocean) and oxic areas (possibly in shallower ocean). When the magnitude of a $\delta^{238}U_{OSW}$ negative excursion is a known fixed value, a higher f^{A}_{inter} baseline requires a larger expansion of euxinia to compensate for the inefficiency of the intermediate reducing sink in burying the heavier ^{238}U isotope during the negative $\delta^{238}U$ shift. As demonstrated in Fig. 3, when the f^{A}_{inter} evolves to decrease by 20% in both scenarios, scenario A with a smaller initial f^{A}_{inter} (30%) requires f^{A}_{eux} to be ca. 10%, whereas scenario B with a larger initial f^{A}_{inter} (60%) requires f^{A}_{eux} to be ca. 23%. In scenario B, the increase in f^{A}_{eux} is comparable to the decrease in f^{A}_{inter}, which is inconsistent with the negative $\delta^{13}C$ shift observed. Considering that the modern deep ocean (water depth >1500 m) comprises 86% of the total ocean area, the intermediate reducing conditions have to be largely distributed in the deep ocean for scenario B with a higher f^{A}_{inter} baseline (60%). In contrast, our preferred scenario A with a lower f^{A}_{inter} baseline (30%) implies relatively limited distribution of intermediate reducing conditions, probably in areas covered by the oldest and most O_2-deficient bottom seawater and/or related with eastern boundary upwelling and thus high primary productivity. Slower ventilation and/or a more efficient biological pump during cooling would have promoted euxinia in those areas.

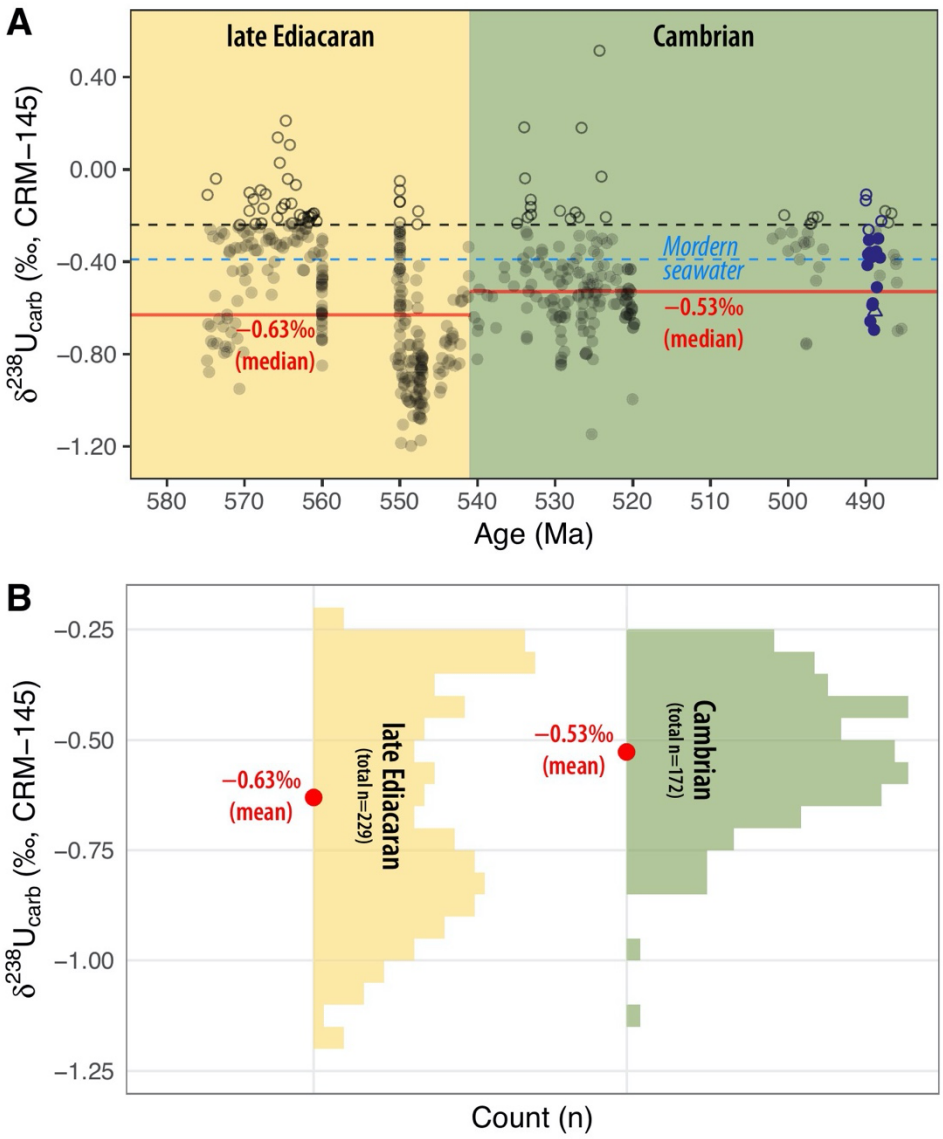

Figure 4: $\delta^{238}U$ in carbonates from late Ediacaran to Cambrian. A) $\delta^{238}U$ data measured in this study are colored in blue. Grey data points are literature data compiled by Chen et al. (2021). Circles are data greater than the riverine input value (−0.24‰, note that the highest estimate compiled by Andersen et al. (2016) is used as the criteria) marked by the black dashed line. The blue dashed line marks the modern seawater value (−0.39‰, Andersen et al., 2016). The red lines are the medians of late Ediacaran and Cambrian, excluding values higher than the riverine input value. B) Probability distribution plots of $\delta^{238}U$ values of late Ediacaran (yellow, n = 229) and Cambrian (green, n = 172), excluding values higher than the riverine input value. The mean $\delta^{238}U$ value (red dots) increased significantly (a one-sided *t*-test yields a *p*-value of 4.4×10^{-7}) from late Ediacaran to Cambrian.

Although the deep ocean can be deoxygenated, both organic carbon burial and intermediate reducing conditions tend to focus towards (on or near) the continental margin, because of higher nutrient availability (from river or eastern boundary upwelling) and higher preservation potential in areas with higher sedimentation rates (Berner, 1982). Therefore, sea level changes can significantly affect the extent of intermediate reducing conditions and the accommodation space for organic carbon burial, and thus contribute to the positive $\delta^{13}C$

458 vs. $\delta^{238}U$ correlation. Such effects could have been more exacerbated during Cambrian Stage 10, because sea
459 level is estimated to be more than 100 m higher than today (Miller et al., 2005), and marginal/epeiric seas
460 were extensive (see the paleogeographic map reconstructed by Scotese (2021) in Fig. 1A).

461 The more doctrinal convergent trends in deep and upper ocean redox conditions during a warming/transgres-
462 sive interval would have increased the extent of both anoxic and intermediate reducing settings, and been re-
463 flected by a more usual negative $\delta^{13}C$ vs. $\delta^{238}U$ correlation, such as observed from the onset of the SPICE
464 (Dahl et al., 2014). However, the upper part of the positive $\delta^{13}C$ shift of SPICE is associated with a positive
465 $\delta^{238}U$ shift and a regression (Saltzman et al., 2000; Dahl et al., 2014; Egenhoff et al., 2015), which is ex-
466 plained by increasing deltaic sinks for both C and U by Dahl et al. (2014). We propose that it may also have
467 been due to oxygenation of former anoxic areas and increasing intermediate reducing settings after massive
468 reductant (organic carbon and pyrite) burial (Gill et al., 2011; Saltzman et al., 2011) and cooling. It is note-
469 worthy that those positive shifts of both $\delta^{13}C$ and $\delta^{238}U$ start with an end-of-biomere extinction, follow an
470 ongoing positive $\delta^{13}C$ shift, and are associated with a regression, while the scenario for the rising limb of
471 TOCE is quite the opposite for all those aspects.

472 ## 4.6. Implications for the terminal Cambrian extinction

473 We propose that the shifts to higher values for both $\delta^{13}C$ and $\delta^{238}U$, following nadirs, at the terminal Cam-
474 brian extinction level, resulted from an expansion of intermediate reducing settings and a concurrent reduc-
475 tion of anoxic (euxinic) settings. This apparently contradicts the traditional hypothesis that anoxia was the
476 'killing mechanism' for the end-of-biomere extinctions. An expansion of persistent anoxic euxinia would
477 have exterminated both shallow- and deeper-water fauna, and inhibited animal diversification (e.g., end-Per-
478 mian extinction). However, such a scenario contradicts the observations that: 1) Benthic faunas and/or biotur-
479 bation occur in worldwide successions during the SPICE interval encompassing the first and second end-of-
480 biomere extinctions (Wotte and Strauss, 2015; Egenhoff et al., 2015); 2) Abundant epifaunal orthid brachio-
481 pods co-occurred with the olenimorphs during the second and third end-of-biomere extinctions (Taylor,
482 2006); 3) All the end-of-biomere extinctions had both high diversification and high extinction rates (Fortey,

1989), and shoreward extending deeper-water benthos, such as olenid trilobites, show a significant higher survival than endemic shelf taxa (Stitt, 1975; Palmer, 1984; Westrop and Ludvigsen, 1987). By contrast, an expansion of intermediate reducing conditions would remove onshore high-O_2-obligatory incumbents, while giving opportunities to the offshore low-O_2-tolerant fauna (Hallam et al., 1989), such as olenimorphs and brachiopods (Farrell et al., 2011). Moreover, intermediate reducing conditions may also reinforce evolutionary innovations (Wood and Erwin, 2018). It is noteworthy that the innovation-promoting 'anoxia', with DO < ~0.5 mL/L and/or dynamic redox, used by Wood and Erwin (2018; see section "II. Low-oxygen habitats: ecology and evolution"), is almost equivalent to the 'intermediate reducing' term used herein, rather than to persistent anoxia or euxinia.

Importantly, the loci of reducing conditions are even more pertinent to the extinctions/turnovers than their areal extents. A negative $\delta^{238}U$ shift is observed to *coincide* with the end-Marjumiid Biomere extinction (Dahl et al., 2014) and *precede* the terminal Cambrian end-Ptychaspid Biomere extinction (this study), respectively, which indicates an expansion of anoxia possibly occurring in the deep ocean for both cases. However, the former case may have also been associated with increasing intermediate reducing conditions killing shelf animals, while animals can still thrive in the oxic shallow ocean for the latter case (similar to the scenario for terminal Ediacaran proposed by Tostevin et al., 2019). The later positive shifts of both $\delta^{13}C$ and $\delta^{238}U$ for the latter case is associated with transgression (Miller et al., 2015), and possibly also warming. Both warming and transgression induce upward and landward movements of OMZ (Riedinger et al. 2021), which may progressively invade the shelf areas and finally trigger the terminal Cambrian extinction. Although the direction of sea-level change at the exact time of the terminal Cambrian extinction is still in dispute (see section 4.3), the invasion of OMZ over the shelf could have been geologically transient and blurred in geological records, but still sufficient to kill.

5. Conclusions

Wa'ergang section $\delta^{238}U$ data, spanning an interval that includes the terminal Cambrian extinction event, exhibit a negative excursion parallel to the TOCE carbon isotope event. This kind of covariation between $\delta^{13}C$

and $\delta^{238}U$ has only rarely been reported and discussed, and is usually attributed to global warming which is inconsistent with evidence for a regression at the nadir of the TOCE. As with other end-of-biomere extinctions, the terminal Cambrian extinction level is associated with a positive $\delta^{13}C$ shift (i.e., rising limb of the TOCE Event). However, unlike some of the end-of-biomere and many major Phanerozoic extinctions, which were also linked to anoxic events based on S (positive $\delta^{34}S$ shift) and/or U (negative $\delta^{238}U$ shift) isotope data, the terminal Cambrian extinction horizon is associated with a positive $\delta^{238}U$ shift, which is generally considered to indicate ocean oxygenation.

Positive $\delta^{13}C$ vs. $\delta^{238}U$ correlation can be explained by intermediate reducing conditions that are likely to have been widespread during the late Cambrian with low atmospheric pO_2 and a greenhouse climate. A higher $\delta^{238}U$ baseline in Cambrian compared with late Ediacaran oceans is consistent with the increasing importance of the intermediate reducing sink.

Coeval negative $\delta^{13}C$ and $\delta^{238}U$ excursions could have driven by divergent trends in deep and upper ocean redox conditions in response to climate changes, as well as the waxing and waning of the accommodation space for organic carbon burial due to sea-level changes. The rising limbs of those isotope excursions, at the terminal Cambrian extinction level, could have resulted from an increase in the intermediate reducing sink for both C and U. An expansion of intermediate reducing settings, rather than anoxic euxinia, is more consistent with the presence of benthic faunas and biogeographical changes associated with not only the terminal Cambrian, but also other late Cambrian end-of-biomere extinctions.

A shift in the $\delta^{238}U$ value indicates a change in the extent of anoxia, it may co-occur with a change in the extent of intermediate reducing conditions. The loci, rather than merely the extents, of those reducing conditions are particularly pertinent to the biotic effects. Therefore, both positive and negative shifts in $\delta^{238}U$ have been linked with extinction events. Progressive understanding about geochemical proxies and the nature of specific biotic events should be combined to keep testing the proposed cause-and-effect linkage between past environmental changes and biological evolution.

Acknowledgements

This research was supported by Natural Science Foundation of China (41603006, 41661134048) and Strategic Priority Research Program (B) of the Chinese Academy of Sciences (XDB26000000). We thank Shan-Chi Peng and Xue-Jian Zhu (NIGPAS) for guidance on fieldwork; Tao Yang (NJU) for help with ICP-MS; Jing Liu (NIGPAS) for carbon isotope analyses; Qian Liu and Pan Sun (NJU) for their assistance in the chemistry lab. Thomas Algeo and an anonymous reviewer provided perceptive and constructive critical comments on the manuscript, and their input significantly improved the manuscript.

References

Abshire, M.L., Romaniello, S.J., Kuzminov, A.M., Cofrancesco, J., Severmann, S., Riedinger, N., 2020. Uranium isotopes as a proxy for primary depositional redox conditions in organic-rich marine systems. Earth Planet. Sci. Lett. 529, 115878. https://doi.org/10.1016/j.epsl.2019.115878

Ahlberg, P., Axheimer, N., Babcock, L.E., Eriksson, M.E., Schmitz, B., Terfelt, F., 2009. Cambrian high-resolution biostratigraphy and carbon isotope chemostratigraphy in Scania, Sweden: first record of the SPICE and DICE excursions in Scandinavia. Lethaia 42, 2–16. https://doi.org/10.1111/j.1502-3931.2008.00127.x

Andersen, M.B., Romaniello, S., Vance, D., Little, S.H., Herdman, R., Lyons, T.W., 2014. A modern framework for the interpretation of $^{238}U/^{235}U$ in studies of ancient ocean redox. Earth Planet. Sci. Lett. 400, 184–194. https://doi.org/10.1016/j.epsl.2014.05.051

Andersen, M.B., Vance, D., Morford, J.L., Bura-Nakic, E., Breitenbach, S.F.M., Och, L., 2016. Closing in on the marine $^{238}U/^{235}U$ budget. Chem. Geol. 420, 11–22. https://doi.org/10.1016/j.chemgeo.2015.10.041

Andersen, M.B., Stirling, C.H., Weyer, S., 2017. Uranium isotope fractionation. Rev. Mineral. Geochem. 82, 799–850. https://doi.org/10.2138/rmg.2017.82.19

Azmy, K., 2019. Carbon-isotope stratigraphy of the uppermost Cambrian in eastern Laurentia: implications for global correlation. Geol. Mag. 156, 759–771. https://doi.org/10.1017/S001675681800002X

Bagnoli, G., Peng, S., Qi, Y., Wang, C., 2017. Conodonts from the Wa'ergang section, China, a potential GSSP for the uppermost stage of the Cambrian. Res. Paleontol. Stratigr. 123. https://doi.org/10.13130/2039-4942/8003

Bartlett, R., Elrick, M., Wheeley, J.R., Polyak, V., Desrochers, A., Asmerom, Y., 2018. Abrupt global-ocean anoxia during the Late Ordovician–early Silurian detected using uranium isotopes of marine carbonates. Proc. Natl. Acad. Sci. U.S.A. 115, 5896–5901. https://doi.org/10.1073/pnas.1802438115

Berner, R.A., 1982. Burial of organic carbon and pyrite sulfur in the modern ocean: Its geochemical and environmental significance. Am. J. Sci. 282, 451–473. https://doi.org/10.2475/ajs.282.4.451

Berner, R.A., 1990. Atmospheric carbon dioxide levels over Phanerozoic time. Science 249, 1382–1386. https://doi.org/10.1126/science.249.4975.1382

Brass, G.W., Southam, J.R., Peterson, W.H., 1982. Warm saline bottom water in the ancient ocean. Nature 296, 620. https://doi.org/10.1038/296620a0

Buggisch, W., Keller, M., Lehnert, O., 2003. Carbon isotope record of Late Cambrian to Early Ordovician carbonates of the Argentine Precordillera. Palaeogeogr., Palaeoclimatol., Palaeoecol. 195, 357–373. https://doi.org/10.1016/S0031-0182(03)00365-1

Bura-Nakić, E., Andersen, M.B., Archer, C., de Souza, G.F., Marguš, M., Vance, D., 2018. Coupled Mo-U abundances and isotopes in a small marine euxinic basin: Constraints on processes in euxinic basins. Geochim. Cosmochim. Acta 222, 212–229. https://doi.org/10.1016/j.gca.2017.10.023

Bura-Nakić, E., Sondi, I., Mikac, N., Andersen, M.B., 2020. Investigating the molybdenum and uranium redox proxies in a modern shallow anoxic carbonate rich marine sediment setting of the Malo Jezero (Mljet Lakes, Adriatic Sea). Chem. Geol. 533, 119441. https://doi.org/10.1016/j.chemgeo.2019.119441

Butterfield, N.J., 2018. Oxygen, animals and aquatic bioturbation: An updated account. Geobiology 16, 3–16. https://doi.org/10.1111/gbi.12267

Chen, J.H., Edwards, R.L., Wasserburg, G.J., 1986. ^{238}U, ^{234}U and ^{232}Th in seawater. Earth Planet. Sci. Lett. 80, 241–251. https://doi.org/10.1016/0012-821X(86)90108-1

Chen, X., Romaniello, S.J., Herrmann, A.D., Wasylenki, L.E., Anbar, A.D., 2016. Uranium isotope fractionation during coprecipitation with aragonite and calcite. Geochim. Cosmochim. Acta 188, 189–207. https://doi.org/10.1016/j.gca.2016.05.022

Chen, X., Tissot, F.L.H., Jansen, M.F., Bekker, A., Liu, C.X., Nie, N.X., Halverson, G.P., Veizer, J., Dauphas, N., 2021. The uranium isotopic record of shales and carbonates through geologic time. Geochim. Cosmochim. Acta 300, 164–191. https://doi.org/10.1016/j.gca.2021.01.040

Clarkson, M.O., Stirling, C.H., Jenkyns, H.C., Dickson, A.J., Porcelli, D., Moy, C.M., Pogge von Strandmann, P.A.E., Cooke, I.R., Lenton, T.M., 2018. Uranium isotope evidence for two episodes of deoxygenation during Oceanic Anoxic Event 2. Proc. Natl. Acad. Sci. U.S.A. 115, 2918–2923. https://doi.org/10.1073/pnas.1715278115

Clarkson, M.O., Müsing, K., Andersen, M.B., Vance, D., 2020. Examining pelagic carbonate-rich sediments as an archive for authigenic uranium and molybdenum isotopes using reductive cleaning and leaching experiments. Chem. Geol. 539, 119412. https://doi.org/10.1016/j.chemgeo.2019.119412

Clarkson, M.O., Lenton, T.M., Andersen, M.B., Bagard, M.-L., Dickson, A.J., Vance, D., 2021. Upper limits on the extent of seafloor anoxia during the PETM from uranium isotopes. Nat. Commun. 12, 399. https://doi.org/10.1038/s41467-020-20486-5

Cole, D.B., Planavsky, N.J., Longley, M., Böning, P., Wilkes, D., Wang, X., Swanner, E.D., Wittkop, C., Loydell, D.K., Busigny, V., Knudsen, A.C., Sperling, E.A., 2020. Uranium isotope fractionation in non-sulfidic anoxic settings and the global uranium isotope mass balance. Global Biogeochem. Cycles 34, e2020GB006649. https://doi.org/10.1029/2020GB006649

Dahl, T.W., Boyle, R.A., Canfield, D.E., Connelly, J.N., Gill, B.C., Lenton, T.M., Bizzarro, M., 2014. Uranium isotopes distinguish two geochemically distinct stages during the later Cambrian SPICE event. Earth Planet. Sci. Lett. 401, 313–326. https://doi.org/10.1016/j.epsl.2014.05.043

Dahl, T.W., Connelly, J.N., Li, D., Kouchinsky, A., Gill, B.C., Porter, S., Maloof, A.C., Bizzarro, M., 2019. Atmosphere–ocean oxygen and productivity dynamics during early animal radiations. Proc. Natl. Acad. Sci. U.S.A. 116, 19352–19361. https://doi.org/10.1073/pnas.1901178116

del Rey, Á., Havsteen, J.C., Bizzarro, M., Dahl, T.W., 2020. Untangling the diagenetic history of uranium isotopes in marine carbonates: A case study tracing the $\delta^{238}U$ composition of late Silurian oceans using calcitic brachiopod shells. Geochim. Cosmochim. Acta 287, 93–110. https://doi.org/10.1016/j.gca.2020.06.002

Dong, X., Zhang, H., 2017. Middle Cambrian through lowermost Ordovician conodonts from Hunan, South China. J. Paleontol. 91, 1–89. https://doi.org/10.1017/jpa.2015.43

Dunk, R.M., Mills, R.A., Jenkins, W.J., 2002. A reevaluation of the oceanic uranium budget for the Holocene. Chem. Geol. 190, 45–67. https://doi.org/10.1016/S0009-2541(02)00110-9

Egenhoff, S.O., Fishman, N.S., Ahlberg, P., Maletz, J., Jackson, A., Kolte, K., Lowers, H., Mackie, J., Newby, W., Petrowsky, M., 2015. Sedimentology of SPICE (Steptoean positive carbon isotope excursion): A high-resolution trace fossil and microfabric analysis of the middle to late Cambrian Alum Shale Formation, southern Sweden, in: Paying Attention to Mudrocks: Priceless! Geological Society of America. https://doi.org/10.1130/2015.2515(05)

Farrell, Ú.C., Briggs, D.E.G., Gaines, R.R., 2011. Paleoecology of the olenid trilobite *triarthrus*: New evidence from beecher's trilobite bed and other sites of pyritization. Palaios 26, 730–742. https://doi.org/10.2110/palo.2011.p11-050r

Fortey, R.A., 1989. There are extinctions and extinctions: examples from the Lower Palaeozoic. Philos. Trans. R. Soc. London, B 325, 327–355. https://doi.org/10.1098/rstb.1989.0092

Frakes, L.A., Francis, J.E., Syktus, J.I., 1992. The Warm Mode: early Cambrian to late Ordovician, in: Climate Modes of the Phanerozoic. Cambridge University Press, pp. 7–14.

Freeman, R.L., Miller, J.F., Dattilo, B.F., 2018. Linguliform brachiopods across a Cambrian–Ordovician (Furongian, Early Ordovician) biomere boundary: the Sunwaptan–Skullrockian North American Stage boundary in the Wilberns and Tanyard formations of central Texas. J. Paleontol. 92, 751–767. https://doi.org/10.1017/jpa.2018.8

Gill, B.C., Lyons, T.W., Young, S.A., Kump, L.R., Knoll, A.H., Saltzman, M.R., 2011. Geochemical evidence for widespread euxinia in the Later Cambrian ocean. Nature 469, 80–83. https://doi.org/10.1038/nature09700

Goto, K.T., Anbar, A.D., Gordon, G.W., Romaniello, S.J., Shimoda, G., Takaya, Y., Tokumaru, A., Nozaki, T., Suzuki, K., Machida, S., Hanyu, T., Usui, A., 2014. Uranium isotope systematics of ferromanganese crusts in the Pacific Ocean: Implications for the marine $^{238}U/^{235}U$ isotope system. Geochim. Cosmochim. Acta 146, 43–58. https://doi.org/10.1016/j.gca.2014.10.003

Guilbaud, R., Slater, B.J., Poulton, S.W., Harvey, T.H.P., Brocks, J.J., Nettersheim, B.J., Butterfield, N.J., 2018. Oxygen minimum zones in the early Cambrian ocean. Geochem. Perspect. Lett. 6, 33–38.

Hallam, A., Cohen, J.M., Chaloner, W.G., 1989. The case for sea-level change as a dominant causal factor in mass extinction of marine invertebrates. Philos. Trans. R. Soc. London, B 325, 437–455. https://doi.org/10.1098/rstb.1989.0098

Harper, D.A.T., Topper, T.P., Cascales-Mi nana, B., Servais, T., Zhang, Y.-D., Ahlberg, P., 2019. The Furongian (late Cambrian) Biodiversity Gap: Real or apparent? Palaeoworld 28, 4–12. https://doi.org/10.1016/j.palwor.2019.01.007

He, Z., Clarkson, M.O., Andersen, M.B., Archer, C., Sweere, T.C., Kraal, P., Guthauser, A., Huang, F., Vance, D., 2021. Temporally and spatially dynamic redox conditions on an upwelling margin: the impact on coupled sedimentary Mo and U isotope systematics, and implications for the Mo-U paleoredox proxy. Geochim. Cosmochim. Acta 309, 251–271. https://doi.org/10.1016/j.gca.2021.06.024

Herrmann, A.D., Gordon, G.W., Anbar, A.D., 2018. Uranium isotope variations in a dolomitized Jurassic carbonate platform (Tithonian; Franconian Alb, Southern Germany). Chem. Geol. 497, 41–53. https://doi.org/10.1016/j.chemgeo.2018.08.017

Hinojosa, J.L., Stirling, C.H., Reid, M.R., Moy, C.M., Wilson, G.S., 2016. Trace metal cycling and $^{238}U/^{235}U$ in New Zealand's fjords: Implications for reconstructing global paleoredox conditions in organic-rich sediments. Geochim. Cosmochim. Acta 179, 89–109. https://doi.org/10.1016/j.gca.2016.02.006

Holmden, C., Amini, M., Francois, R., 2015. Uranium isotope fractionation in Saanich Inlet: A modern analog study of a paleoredox tracer. Geochim. Cosmochim. Acta 153, 202–215. https://doi.org/10.1016/j.gca.2014.11.012

Jaccard, S.L., Galbraith, E.D., 2012. Large climate-driven changes of oceanic oxygen concentrations during the last deglaciation. Nat. Geosci. 5, 151–156. https://doi.org/10.1038/ngeo1352

Jost, A.B., Bachan, A., van de Schootbrugge, B., Lau, K.V., Weaver, K.L., Maher, K., Payne, J.L., 2017. Uranium isotope evidence for an expansion of marine anoxia during the end-Triassic extinction. Geochem., Geophys., Geosyst. 18, 3093–3108. https://doi.org/10.1002/2017GC006941

Kaufman, A.J., Knoll, A.H., 1995. Neoproterozoic variations in the C-isotopic composition of seawater: Stratigraphic and biogeochemical implications. Precambrian Res. 73, 27–49. https://doi.org/10.1016/0301-9268(94)00070-8

Krause, A.J., Mills, B.J.W., Zhang, S., Planavsky, N.J., Lenton, T.M., Poulton, S.W., 2018. Stepwise oxygenation of the Paleozoic atmosphere. Nat. Commun. 9, 4081. https://doi.org/10.1038/s41467-018-06383-y

Landing, E., 2011. No Late Cambrian shoreline ice in Laurentia. GSA Today 21, e19. https://doi.org/10.1130/G113C.1

Landing, E., Westrop, S.R., Adrain, J.M., 2011. The Lawsonian Stage - the *Eoconodontus notchpeakensis* FAD and HERB carbon isotope excursion define a globally correlatable terminal Cambrian stage. Bull. Geosci. 86, 621–640.

Landing, E., 2012. Time-specific black mudstones and global hyperwarming on the Cambrian–Ordovician slope and shelf of the Laurentia palaeocontinent. Palaeogeogr., Palaeoclimatol., Palaeoecol. 367–368, 256–272. https://doi.org/10.1016/j.palaeo.2011.09.005

Landing, E., Ripperdan, R.L., Geyer, G., 2020. Uppermost Cambrian carbon chemostratigraphy: the HERB and undocumented TOCE events are not synonymous. Geol. Mag. 157, 1373–1377. https://doi.org/10.1017/S0016756820000382

Lau, K.V., Maher, K., Altiner, D., Kelley, B.M., Kump, L.R., Lehrmann, D.J., Silva-Tamayo, J.C., Weaver, K.L., Yu, M., Payne, J.L., 2016. Marine anoxia and delayed Earth system recovery after the end-Permian extinction. Proc. Natl. Acad. Sci. U.S.A. 113, 2360–2365. https://doi.org/10.1073/pnas.1515080113

Lau, K.V., Macdonald, F.A., Maher, K., Payne, J.L., 2017. Uranium isotope evidence for temporary ocean oxygenation in the aftermath of the Sturtian Snowball Earth. Earth Planet. Sci. Lett. 458, 282–292. https://doi.org/10.1016/j.epsl.2016.10.043

Lau, K.V., Lyons, T.W., Maher, K., 2020. Uranium reduction and isotopic fractionation in reducing sediments: Insights from reactive transport modeling. Geochim. Cosmochim. Acta 287, 65–92. https://doi.org/10.1016/j.gca.2020.01.021

Li, D., Zhang, X., Chen, K., Zhang, G., Chen, X., Huang, W., Peng, S., Shen, Y., 2017. High-resolution C-isotope chemostratigraphy of the uppermost Cambrian stage (Stage 10) in South China: implications for defining the base of Stage 10 and palaeoenvironmental change. Geol. Mag. 154, 1232–1243. https://doi.org/10.1017/S0016756817000188

Loch, J.D., Stitt, J.H., Derby, J.R., 1993. Cambrian–Ordovician boundary interval extinctions: implications of revised trilobite and brachiopod data from Mount Wilson, Alberta, Canada. J. Paleontol. 67, 497–517. https://doi.org/10.1017/S0022336000024859

Matsumoto, K., 2007. Biology-mediated temperature control on atmospheric pCO_2 and ocean biogeochemistry. Geophys. Res. Lett. 34. https://doi.org/10.1029/2007GL031301

McLennan, S.M., 2001. Relationships between the trace element composition of sedimentary rocks and upper continental crust. Geochem., Geophys., Geosyst. 2. https://doi.org/10.1029/2000GC000109

Miller, K.G., Kominz, M.A., Browning, J.V., Wright, J.D., Mountain, G.S., Katz, M.E., Sugarman, P.J., Cramer, B.S., Christie-Blick, N., Pekar, S.F., 2005. The Phanerozoic record of global sea-level change. Science 310, 1293–1298. https://doi.org/10.1126/science.1116412

Miller, J.F., Ethington, R.L., Evans, K.R., Holmer, L.E., Loch, J.D., Popov, L.E., Repetski, J.E., Ripperdan, R.L., Taylor, J.F., 2006. Proposed stratotype for the base of the highest Cambrian stage at the first appearance datum of *Cordylodus andresi*, Lawson Cove section, Utah, USA. Palaeoworld 15, 384–405. https://doi.org/10.1016/j.palwor.2006.10.017

Miller, J.F., Ripperdan, R.L., Loch, J.D., Freeman, R.L., Evans, K.R., Taylor, J.F., Tolbart, Z.C., 2015. Proposed GSSP for the base of Cambrian Stage 10 at the lowest occurrence of *Eoconodontus notchpeakensis* in the House Range, Utah, USA. Annales de Paléontologie 101, 199–211. https://doi.org/10.1016/j.annpal.2015.04.008

713 Morford, J.L., Emerson, S.R., Breckel, E.J., Kim, S.H., 2005. Diagenesis of oxyanions (V, U, Re, and Mo) in
714 pore waters and sediments from a continental margin. Geochim. Cosmochim. Acta 69, 5021–5032.
715 https://doi.org/10.1016/j.gca.2005.05.015
716 Palmer, A.R., 1965. Biomere: A new kind of biostratigraphic unit. J. Paleontol. 39, 149–153.
717 Palmer, A.R., 1984. The biomere problem: Evolution of an idea. J. Paleontol. 58, 599–611.
718 Peng, S., Babcock, L.E., Cooper, R.A., 2012. The Cambrian Period, in: Gradstein, F.M., Ogg, J.G., Schmitz,
719 M.D., Ogg, G.M. (Eds.), The Geologic Time Scale 2012. Elsevier, pp. 437–488.
720 Peng, S., Babcock, L.E., Zhu, X., Zuo, J., Dai, T., 2014. A potential GSSP for the base of the uppermost
721 Cambrian stage, coinciding with the first appearance of *Lotagnostus americanus* at Wa'ergang, Hunan,
722 China. GFF 136, 208–213. https://doi.org/10.1080/11035897.2013.865666
723 Pohl, A., Lu, Z., Lu, W., Stockey, R.G., Elrick, M., Li, M., Desrochers, A., Shen, Y., He, R., Finnegan, S.,
724 Ridgwell, A., 2021. Vertical decoupling in Late Ordovician anoxia due to reorganization of ocean cir-
725 culation. Nat. Geosci. In Press. https://doi.org/10.1038/s41561-021-00843-9
726 Railsback, L.B., Ackerly, S.C., Anderson, T.F., Cisneti, J.L., 1990. Palaeontological and isotope evidence for
727 warm saline deep waters in Ordovician oceans. Nature 343, 156. https://doi.org/10.1038/343156a0
728 Riedinger, N., Scholz, F., Abshire, M.L., Zabel, M., 2021. Persistent deep water anoxia in the eastern South
729 Atlantic during the last ice age. Proc. Natl. Acad. Sci. U.S.A. 118.
730 https://doi.org/10.1073/pnas.2107034118
731 Ripperdan, R.L., Magaritz, M., Nicoll, R.S., Shergold, J.H., 1992. Simultaneous changes in carbon isotopes,
732 sea level, and conodont biozones within the Cambrian-Ordovician boundary interval at Black Moun-
733 tain, Australia. Geology 20, 1039–1042. https://doi.org/10.1130/0091-7613(1992)020<1039:SCI-
734 CIS>2.3.CO;2
735 Ripperdan, R.L., Magaritz, M., Kirschvink, J.L., 1993. Carbon isotope and magnetic polarity evidence for
736 non-depositional events within the Cambrian–Ordovician boundary section near Dayangcha, Jilin Prov-
737 ince, China. Geological Magazine 130, 443–452. https://doi.org/10.1017/S0016756800020525
738 Ripperdan, R.L., 2002. The HERB event: End of Cambrian carbon cycle paradigm? in: Geol. Soc. Am. Pro-
739 grams Abstracts. p. 413.

740 Romaniello, S.J., Herrmann, A.D., Anbar, A.D., 2013. Uranium concentrations and $^{238}U/^{235}U$ isotope ratios
741 in modern carbonates from the Bahamas: Assessing a novel paleoredox proxy. Chem. Geol. 362, 305–
742 316. https://doi.org/10.1016/j.chemgeo.2013.10.002
743 Runkel, A.C., Mackey, T.J., Cowan, C.A., Fox, D.L., 2010. Tropical shoreline ice in the late Cambrian:
744 Implications for Earth's climate between the Cambrian Explosion and the Great Ordovician
745 Biodiversification Event. GSA Today 20, 4–10. https://doi.org/10.1130/GSATG84A.1
746 Saltzman, M.R., Davidson, J.P., Holden, P., Runnegar, B., Lohmann, K.C., 1995. Sea-level-driven changes
747 in ocean chemistry at an Upper Cambrian extinction horizon. Geology 23, 893–896.
748 https://doi.org/10.1130/0091-7613(1995)023<0893:SLDCIO>2.3.CO;2
749 Saltzman, M.R., Ripperdan, R.L., Brasier, M.D., Lohmann, K.C., Robison, R.A., Chang, W.T., Peng, S.,
750 Ergaliev, E.K., Runnegar, B., 2000. A global carbon isotope excursion (SPICE) during the Late
751 Cambrian: relation to trilobite extinctions, organic-matter burial and sea level. Palaeogeogr.,
752 Palaeoclimatol., Palaeoecol. 162, 211–223. https://doi.org/10.1016/S0031-0182(00)00128-0
753 Saltzman, M.R., Young, S.A., Kump, L.R., Gill, B.C., Lyons, T.W., Runnegar, B., 2011. Pulse of atmos-
754 pheric oxygen during the late Cambrian. Proc. Natl. Acad. Sci. U.S.A. 108, 3876–3881.
755 https://doi.org/10.1073/pnas.1011836108
756 Saltzman, M.R., Edwards, C.T., Adrain, J.M., Westrop, S.R., 2015. Persistent oceanic anoxia and elevated
757 extinction rates separate the Cambrian and Ordovician radiations. Geology 43, 807–810.
758 https://doi.org/10.1130/G36814.1
759 Schlesinger, W.H., Melack, J.M., 1981. Transport of organic carbon in the world's rivers. Tellus 33, 172–
760 187. https://doi.org/10.3402/tellusa.v33i2.10706
761 Scotese, C.R., 2021. An atlas of Phanerozoic paleogeographic maps: The seas come in and the seas go out.
762 Annu. Rev. Earth Planet. Sci. 49, 679–728. https://doi.org/10.1146/annurev-earth-081320-064052
763 Sheehan, P.M., 2001. History of marine biodiversity. Geol. J. 36, 231–249. https://doi.org/10.1002/gj.890
764 Sial, A.N., Peralta, S., Gaucher, C., Toselli, A.J., Ferreira, V.P., Frei, R., Parada, M.A., Pimentel, M.M., Pe-
765 reira, N.S., 2013. High-resolution stable isotope stratigraphy of the upper Cambrian and Ordovician in

766 the Argentine Precordillera: Carbon isotope excursions and correlations. Gondwana Res. 24, 330–348.
767 https://doi.org/10.1016/j.gr.2012.10.014
768 Sigman, D.M., Hain, M.P., Haug, G.H., 2010. The polar ocean and glacial cycles in atmospheric CO_2 con-
769 centration. Nature 466, 47. https://doi.org/10.1038/nature09149
770 Stirling, C.H., Andersen, M.B., Potter, E.-K., Halliday, A.N., 2007. Low-temperature isotopic fractionation
771 of uranium. Earth Planet. Sci. Lett. 264, 208–225. https://doi.org/10.1016/j.epsl.2007.09.019
772 Stitt, J.H., 1971. Repeating evolutionary pattern in late Cambrian trilobite biomeres. J. Paleontol. 45, 178–
773 181.
774 Stitt, J.H., 1975. Adaptive radiation, trilobite paleoecology, and extinction, Ptychaspidid Biomere, Late Cam-
775 brian of Oklahoma. Fossils Strata 4, 381–390.
776 Taylor, J.F., 2006. History and status of the biomere concept. Mem. Assoc. Australas. Palaeontol. 247–265.
777 Tostevin, R., Clarkson, M.O., Gangl, S., Shields, G.A., Wood, R.A., Bowyer, F., Penny, A.M., Stirling, C.H.,
778 2019. Uranium isotope evidence for an expansion of anoxia in terminal Ediacaran oceans. Earth Planet.
779 Sci. Lett. 506, 104–112. https://doi.org/10.1016/j.epsl.2018.10.045
780 Trotter, J.A., Williams, I.S., Barnes, C.R., Lécuyer, C., Nicoll, R.S., 2008. Did cooling oceans trigger Ordo-
781 vician biodiversification? Evidence from conodont thermometry. Science 321, 550–554.
782 https://doi.org/10.1126/science.1155814
783 Tyson, R.V., Pearson, T.H., 1991. Modern and ancient continental shelf anoxia: An overview. Geol. Soc.,
784 London, Spec. Publ. 58, 1–24. https://doi.org/10.1144/GSL.SP.1991.058.01.01
785 Westrop, S.R., Ludvigsen, R., 1987. Biogeographic control of trilobite mass extinction at an upper Cambrian
786 “biomere” boundary. Paleobiology 13, 84–99.
787 Weyer, S., Anbar, A.D., Gerdes, A., Gordon, G.W., Algeo, T.J., Boyle, E.A., 2008. Natural fractionation of
788 $^{238}U/^{235}U$. Geochim. Cosmochim. Acta 72, 345–359. https://doi.org/10.1016/j.gca.2007.11.012
789 White, D.A., Elrick, M., Romaniello, S., Zhang, F., 2018. Global seawater redox trends during the Late De-
790 vonian mass extinction detected using U isotopes of marine limestones. Earth Planet. Sci. Lett. 503,
791 68–77. https://doi.org/10.1016/j.epsl.2018.09.020

792 Wood, R., Erwin, D.H., 2018. Innovation not recovery: dynamic redox promotes metazoan radiations. Biol.
793 Rev. 93, 863–873. https://doi.org/10.1111/brv.12375
794 Wotte, T., Strauss, H., 2015. Questioning a widespread euxinia for the Furongian (Late Cambrian) SPICE
795 event: indications from $\delta^{13}C$, $\delta^{18}O$, $\delta^{34}S$ and biostratigraphic constraints. Geol. Mag. 152, 1085–1103.
796 https://doi.org/10.1017/S0016756815000187
797 Zhang, F., Algeo, T.J., Romaniello, S.J., Cui, Y., Zhao, L., Chen, Z.-Q., Anbar, A.D., 2018a. Congruent Per-
798 mian-Triassic $\delta^{238}U$ records at Panthalassic and Tethyan sites: Confirmation of global-oceanic anoxia
799 and validation of the U-isotope paleoredox proxy. Geology 46, 327. https://doi.org/10.1130/G39695.1
800 Zhang, F., Xiao, S., Kendall, B., Romaniello, S.J., Cui, H., Meyer, M., Gilleaudeau, G.J., Kaufman, A.J.,
801 Anbar, A.D., 2018b. Extensive marine anoxia during the terminal Ediacaran Period. Sci. Adv. 4.
802 https://doi.org/10.1126/sciadv.aan8983
803 Zhang, F., Algeo, T.J., Cui, Y., Shen, J., Song, H., Sano, H., Rowe, H.D., Anbar, A.D., 2019. Global-ocean
804 redox variations across the Smithian-Spathian boundary linked to concurrent climatic and biotic
805 changes. Earth-Sci. Rev. 195, 147–168. https://doi.org/10.1016/j.earscirev.2018.10.012
806 Zhang, F., Shen, S., Cui, Y., Lenton, T.M., Dahl, T.W., Zhang, H., Zheng, Q., Wang, W., Krainer, K., Anbar,
807 A.D., 2020. Two distinct episodes of marine anoxia during the Permian-Triassic crisis evidenced by
808 uranium isotopes in marine dolostones. Geochim. Cosmochim. Acta 287, 165–179.
809 https://doi.org/10.1016/j.gca.2020.01.032
810 Zheng, Y., Anderson, R.F., Geen, A. van, Fleisher, M.Q., 2002. Preservation of particulate non-lithogenic
811 uranium in marine sediments. Geochim. Cosmochim. Acta 66, 3085–3092.
812 https://doi.org/10.1016/S0016-7037(01)00632-9
813 Zhu, M.-Y., Babcock, L.E., Peng, S.-C., 2006. Advances in Cambrian stratigraphy and paleontology: Inte-
814 grating correlation techniques, paleobiology, taphonomy and paleoenvironmental reconstruction. Palae-
815 oworld 15, 217–222. https://doi.org/10.1016/j.palwor.2006.10.016
816 Zhu, M., Babcock, L.E., Peng, S., Ahlberg, P., 2021. Reply to 'Uppermost Cambrian carbon chemostratigra-
817 phy: the HERB and undocumented TOCE events are not synonymous'. Geol. Mag. 158, 1323–1326.
818 https://doi.org/10.1017/S0016756820001120

819 Zhuravlev, A.Yu., 2001. Biotic Diversity and Structure During the Neoproterozoic–Ordovician Transition,
820 in: Zhuravlev, A., Riding, R. (Eds.), The Ecology of the Cambrian Radiation. Columbia University
821 Press.
822